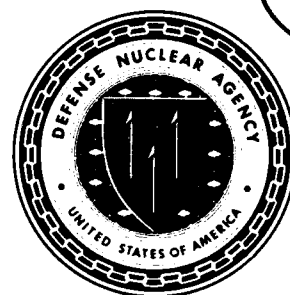


AD-A218 046



DTIC FILE COPY

Defense Nuclear Agency
Alexandria, VA 22310-3398



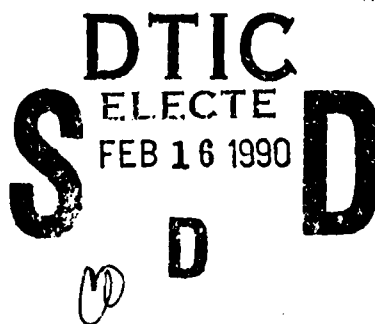
DNA-TR-88-212

Role of Soil Hysteresis in Impedance Testing as Applied to Buried Arches

R. S. Atkatsch
Weidlinger Associates, Inc.
333 Seventh Avenue
New York, NY 10001

February 1990

Technical Report



CONTRACT No. DNA 001-85-C-0413

Approved for public release;
distribution is unlimited.

90 02 15 004

Destroy this report when it is no longer needed. Do not return to sender.

PLEASE NOTIFY THE DEFENSE NUCLEAR AGENCY,
ATTN: CSTI, 6801 TELEGRAPH ROAD, ALEXANDRIA, VA
22310-3398, IF YOUR ADDRESS IS INCORRECT, IF YOU
WISH IT DELETED FROM THE DISTRIBUTION LIST, OR
IF THE ADDRESSEE IS NO LONGER EMPLOYED BY YOUR
ORGANIZATION.



DISTRIBUTION LIST UPDATE

This mailer is provided to enable DNA to maintain current distribution lists for reports. We would appreciate your providing the requested information.

- ☐ Add the individual listed to your distribution list.
- ☐ Delete the cited organization/individual.
- ☐ Change of address.

NAME: _____

ORGANIZATION: _____

OLD ADDRESS

CURRENT ADDRESS

TELEPHONE NUMBER: () _____

SUBJECT AREA(s) OF INTEREST:

DNA OR OTHER GOVERNMENT CONTRACT NUMBER: _____

CERTIFICATION OF NEED-TO-KNOW BY GOVERNMENT SPONSOR (if other than DNA):

SPONSORING ORGANIZATION: _____

CONTRACTING OFFICER OR REPRESENTATIVE: _____

SIGNATURE: _____

CUT HERE AND RETURN



REPORT DOCUMENTATION PAGE

1a. REPORT SECURITY CLASSIFICATION UNCLASSIFIED			1b. RESTRICTIVE MARKINGS		
2a. SECURITY CLASSIFICATION AUTHORITY N/A since Unclassified			3. DISTRIBUTION/AVAILABILITY OF REPORT Approved for public release; distribution is unlimited.		
2b. DECLASSIFICATION/DOWNGRADING SCHEDULE N/A since Unclassified					
4. PERFORMING ORGANIZATION REPORT NUMBER(S) WA 8810			5. MONITORING ORGANIZATION REPORT NUMBER(S) DNA-TR-88-212		
6a. NAME OF PERFORMING ORGANIZATION Weidlinger Associates, Inc.		6b. OFFICE SYMBOL (If applicable)		7a. NAME OF MONITORING ORGANIZATION Defense Nuclear Agency	
6c. ADDRESS (City, State, and ZIP Code) 333 Seventh Avenue New York, NY 10001			7b. ADDRESS (City, State, and ZIP Code) 6801 Telegraph Road Alexandria, VA 22310-3398		
8a. NAME OF FUNDING/SPONSORING ORGANIZATION		8b. OFFICE SYMBOL (If applicable) SPSD/McDugald		9. PROCUREMENT INSTRUMENT IDENTIFICATION NUMBER DNA 001-85-C-0413	
9c. ADDRESS (City, State, and ZIP Code)			10. SOURCE OF FUNDING NUMBERS		
			PROGRAM ELEMENT NO. 62715H	PROJECT NO. S	TASK NO. C
			WORK UNIT ACCESSION NO. DH009196		
11. TITLE (Include Security Classification) Role of Soil Hysteresis in Impedance Testing as Applied to Buried Arches					
12. PERSONAL AUTHOR(S) Atkatsh, R. S.					
13a. TYPE OF REPORT Technical		13b. TIME COVERED FROM 860218 TO 881031		14. DATE OF REPORT (Year, Month, Day) 900201	
15. PAGE COUNT 34					
16. SUPPLEMENTARY NOTATION This work was sponsored by the Defense Nuclear Agency under RDT&E RMC Code B344085466 S C 00104 25904D.					
17. COSATI CODES			18. SUBJECT TERMS (Continue on reverse if necessary and identify by block number)		
FIELD	GROUP	SUB-GROUP			
8	7		Structure-Medium Interaction		
13	13		Finite Element Simulation		
			Hysteretic Damping		
19. ABSTRACT (Continue on reverse if necessary and identify by block number) The effect of backfill soil hysteretic damping upon the suppression of resonance for buried arches is examined. Finite element simulation of a buried arch structure shows that the backfill soil hysteretic behavior is a dominant factor in explaining the absence of resonance in arch tests. <i>Keywords.</i>					
20. DISTRIBUTION/AVAILABILITY OF ABSTRACT <input type="checkbox"/> UNCLASSIFIED/UNLIMITED <input checked="" type="checkbox"/> SAME AS RPT <input type="checkbox"/> DTIC USERS			21. ABSTRACT SECURITY CLASSIFICATION UNCLASSIFIED		
22a. NAME OF RESPONSIBLE INDIVIDUAL Bennie F. Maddox			22b. TELEPHONE (Include Area Code) (703) 325-7042		22c. OFFICE SYMBOL DNA/CSTI

CONVERSION TABLE

Conversion factors for U.S. customary
to metric (SI) units of measurement

To Convert From	To	Multiply By
angstrom	meters (m)	1.000 000 X E -10
atmosphere (normal)	kilo pascal (kPa)	1.013 25 X E +2
bar	kilo pascal (kPa)	1.000 000 X E +2
barn	meter ² (m ²)	1.000 000 X E -28
British Thermal unit (thermochemical)	joule (J)	1.054 350 X E +3
calorie (thermochemical)	joule (J)	4.184 000
cal (thermochemical)/cm ²	mega joule/m ² (MJ/m ²)	4.184 000 X E -2
curie	giga becquerel (GBq)*	3.700 000 X E +1
degree (angle)	radian (rad)	1.745 329 X E -2
degree Fahrenheit	degree kelvin (K)	$T_K = (t^{\circ}F + 459.67)/1.8$
electron volt	joule (J)	1.602 19 X E -19
erg	joule (J)	1.000 000 X E -7
erg/second	watt (W)	1.000 000 X E -7
foot	meter (m)	3.048 000 X E -1
foot-pound-force	joule (J)	1.355 818
gallon (U.S. liquid)	meter ³ (m ³)	3.785 412 X E -3
inch	meter (m)	2.540 000 X E -2
jerk	joule (J)	1.000 000 X E +9
joule/kilogram (J/kg) (radiation dose absorbed)	Gray (Gy)**	1.000 000
kilotons	terajoules	4.183
kip (1000 lbf)	newton (N)	4.448 222 X E +3
kip/inch ² (ksi)	kilo pascal (kPa)	6.894 757 X E +3
ktop	newton-second/m ² (N-s/m ²)	1.000 000 X E +2
micron	meter (m)	1.000 000 X E -6
mil	meter (m)	2.540 000 X E -5
mile (international)	meter (m)	1.609 344 X E +3
ounce	kilogram (kg)	2.834 952 X E -2
pound-force (lbf avoirdupois)	newton (N)	4.448 222
pound-force inch	newton-meter (N·m)	1.129 848 X E -1
pound-force/inch	newton/meter (N/m)	1.751 268 X E +2
pound-force/foot ²	kilo pascal (kPa)	4.788 026 X E -2
pound-force/inch ² (psi)	kilo pascal (kPa)	6.894 757
pound-mass (lbm avoirdupois)	kilogram (kg)	4.535 924 X E -1
pound-mass-foot ² (moment of inertia)	kilogram-meter ² (kg·m ²)	4.214 011 X E -2
pound-mass/foot ³	kilogram/meter ³ (kg/m ³)	1.601 846 X E +1
rad (radiation dose absorbed)	Gray (Gy)**	1.000 000 X E -2
roentgen	coulomb/kilogram (C/kg)	2.579 160 X E -4
shake	second (s)	1.000 000 X E -8
slug	kilogram (kg)	1.459 390 X E +1
torr (mm Hg, 0°C)	kilo pascal (kPa)	1.333 22 X E -1

*The becquerel (Bq) is the SI unit of radioactivity; Bq = 1 event/s.

**The Gray (Gy) is the SI unit of absorbed radiation.

TABLE OF CONTENTS

Section	Page
COVERSION TABLE	iii
FIGURES	v
1 INTRODUCTION	1
1.1 BACKGROUND	1
1.2 SCOPE AND OBJECTIVES	1
1.3 IMPEDANCE TESTING: METHODOLOGY AND RESULTS ..	2
2 SIMULATION OF BURIED ARCH STRUCTURES	4
2.1 FINITE ELEMENT METHODOLOGY	4
2.2 VISCOELASTIC CAP MODEL	5
3 RESULTS OF BURIED ARCH SIMULATION STUDIES	8
3.1 DISCUSSION OF RESULTS	8
4 CONCLUSIONS AND RECOMMENDATIONS	11
4.1 CONCLUSIONS	11
4.2 RECOMMENDATIONS	11
5 REFERENCES	12
NOTATION	25

FIGURES

Figure		Page
1	Geometry and instrumentation for arch structure	13
2	Finite element model of buried arch	14
3	Uniaxial stress-strain properties of compacted native backfill ESSEX V arch	15
4	ARCH structure 3A, analytical response at crown—single vibration test, F1 = 500 lbs	16
5	Elastic soil cap model—ARCH structure 3A, analytical response at crown—single vibration test, F1 = 500 lbs	17
6	Hysteretic soil cap model—ARCH structure 3A, analytical responses at crown—single vibration test, F1 = 500 lbs	18
7	ARCH structure 3A, analytical response at gage location A3, single vibration test, F1 = 500 lbs	19
8	Elastic soil cap model—ARCH structure 3A, response data at gage A3—two vibrators in phase, F2 = F3 = 500 lbs	20
9	Hysteretic soil cap model—ARCH structure 3A, response data at gage A3—two vibrators in phase, F2 = F3 = 500 lbs	21
10	ARCH structure 3A, analytical response at gage location A3, two vibrators out of phase, F2 = F3 = 500 lbs	22
11	Elastic soil cap model—ARCH structure 3A, response data at gage A3—two vibrators out of phase test, F2 = F3 = 500 lbs	23
12	Hysteretic soil cap model—ARCH structure 3A, response data at gage A3—two vibrators out of phase test, F2 = F3 = 500 lbs	24

Accession For	
NTIS CRA&I	<input checked="" type="checkbox"/>
DTIC TAB	<input type="checkbox"/>
Unannounced	<input type="checkbox"/>
Justification	
By	
Distribution	
Availability	
Dist	Special
A-1	

SECTION 1

INTRODUCTION

1.1 BACKGROUND.

The use of impedance testing and its application to buried arch response is discussed in this report. A goal of impedance testing is to produce functional relations which characterize the shock input levels at points of equipment attachment to the structure. The experimentally determined impedances of the structure are used to develop a transfer function between the generalized input loads upon the structure and the dynamic response velocities at the attachment points of equipment. The restriction of this methodology is that linear behavior of both the structure and the soil must exist. The reality is that some degree of nonlinearity occurs at any significant pressure level with the onset of soil nonlinearity preceding the onset of structural nonlinearity.

The particular impedance tests studied in this report are the forced vibration tests performed on uncovered and shallow buried arch and rectangular structures in the ESSEX V Phase 3 test series. (Ref. 1)

For these tests, the original backfill was excavated and the uncovered structure was subjected to forced vibration tests. The sand backfill was then replaced by raining it from a height of five feet and the forced vibration tests were repeated. Figure 1 shows the geometry of the arch structure and the backfill and instrumentation layout.

Test results include impedance (F_{max}/V_{max}) versus frequency relationships. Resonance is defined to occur when the driving frequency approaches a particular natural frequency of the structure. This is exhibited by a valley in the impedance versus frequency curve.

The test results showed that for the rectangular structures, resonance was observed in the shallow buried structures at the same frequencies as in the uncovered box structure. For the arch structure, resonance was not experimentally observed in the shallow buried arches.

In an attempt to explain the differences in the experimental results of the boxes and the arches, linear time domain analyses were previously performed to simulate the behavior of these structures (Ref. 2). These analyses examined what levels of radiation damping would be needed to suppress resonance. It was determined that for the box structure, radiation damping of the order of 10% to 20% was needed to suppress resonance. For the arch structure, it was determined that a radiation damping level of 50% would be needed to suppress damping. Since measured values of radiation damping are in the range of 10 to 15%, it was concluded that radiation damping alone could not account for the suppression of damping for the covered arches.

Identified in Ref. 2 as an additional damping source was hysteretic behavior in the soil adjacent to the structure. Hysteresis in soil stress-strain relations describes the energy losses produced by the load/unload and reload cycles. These cycles are produced in the soil by the driving oscillations of the buried structure. The contributing effect of the soil hysteresis upon the experimentally observed suppression of arch resonance will be further discussed in this report.

1.2 SCOPE AND OBJECTIVES.

This report discusses the development and validation of analytical techniques for hardness assessment of shallow buried arches. It represents an extension of previous studies done by

Weidlinger Associates under DNA Sponsorship to simulate the forced vibration testing of uncovered and covered arches and boxes in Project ESSEX. Those studies indicated that material and geometrical non-linearities needed to be considered when modeling shallow buried arches.

The role of the various component soil material non-linearities and their interplay with the arch structure is examined in this report. Particular attention is drawn to the responsibility of soil non-linearities in helping to describe the appreciable difference between the shallow buried arch and box behavior.

Time marching simulation using non-linear finite element analysis is performed to overcome the theoretical obstacle presented by the non-linear soil-structure system. Various analytical models of the soil media are used to isolate the influences of soil behavior upon the response of buried arches to impedance testing.

The examination of soil response is within the scope of the study of impedance testing as applied to buried arches. Determining the extent of non-linear soil response will greatly aid the investigation to determine the extent non-linearities render the impedance technique impractical for shallow buried arches. This study will also assist in the development of analytical techniques which utilize the results of impedance testing to develop shock input levels at equipment attachment points.

1.3 IMPEDANCE TESTING: METHODOLOGY AND RESULTS.

The use of impedance testing and its application to buried arch response is discussed in this report. A goal of impedance testing is to produce functional relations which characterize the shock input levels at points of equipment attachment to the structure. The experimentally determined impedances of the structure are used to develop a transfer function between the

generalized input loads upon the structure and the dynamic response velocities at the attachment points of equipment. The restriction on this methodology is that linear behavior of both the structure and the soil must exist. The reality is that some degree of nonlinearity occurs at any significant pressure level with the onset of soil nonlinearity preceding the onset of structural nonlinearity.

Impedances are measured by applying an input forcing function to the structure using either electromagnetic (low force and high frequency) or electro hydraulic (high force, low frequency) vibrators. A variable sine sweep rate is used when driving the structure. The impedance is determined using a measurement point and a series of drive points on the structure. The response of the measurement point to different driving frequencies is found by summing the products of experimentally determined impedance functions and drive functions in the frequency domain.

The particular impedance tests studied in this report are the forced vibration tests performed on uncovered and shallow buried arch and rectangular structures in the ESSEX V Phase 3 test series. Constant force sinusoidal frequency sweeps were run at three different force levels. Mechanical impedance (F_{max}/V_{max}) versus frequency plots were made. Resonant frequencies were determined from such system curves. An outline of the test plan for ARCH 3A (Covered and Uncovered) is below.

The test results obtained showed that for the rectangular structures, resonance was observed in the shallow buried structures at the same frequencies as in the uncovered box structures. For the arch structures, resonance was not experimentally observed in the shallow buried arch structures. In an attempt to explain the differences in the experimental results of the boxes and the arches, analyses were performed to simulate the behavior of certain types of

shallow buried structures subjected to forced vibration testing. (Refs. 2,3 and 4).

<u>TEST DESCRIPTION</u>	<u>DRIVE POINT</u>	<u>FORCING FUNCTION</u>
SINGLE VIBRATOR	F1	FREQUENCY SWEEP
DUAL VIBRATORS IN PHASE	F2 and F3	FREQUENCY SWEEP IN PHASE
DUAL VIBRATORS OUT OF PHASE	F2 and F3	FREQUENCY SWEEP OUT OF PHASE

SECTION 2

SIMULATION OF BURIED ARCH STRUCTURES

2.1 FINITE ELEMENT METHODOLOGY.

The finite element method together with an explicit central difference integration scheme is utilized in the analysis of shallow buried arches subjected to dynamic loading. Both material and geometrical nonlinearities are considered in the analysis.

The plane strain finite element program SADNESS (SEISMIC ANALYSIS for DYNAMIC NONLINEAR SLOPE STABILITY) (Ref. 5) is used. The SADNESS program was developed to examine the earthquake induced failure of earth slopes. Its range of applicability includes the non-linear response of buried structures subjected to vibrational loadings. Both geometrical and material nonlinearities are accounted for. Geometrical nonlinearities are incorporated through the use of an incrementally updated Lagrangian approach in conjunction with a constitutive equation relating the co-rotational stress rate to the rate of deformation tensor. The theory is valid for large deformations (strains) as well as for large deflections and rotations. Material nonlinearities are incorporated through the use of a cap model constitutive model extended to improve its capability to represent cyclic behavior characteristic of sinusoidal ground motions.

The SADNESS model of the buried arch (Figure 2) consisted of 455 elements and 267 nodal points. Constant strain triangles are used throughout. Five (5) different materials were modelled including the concrete arch, the backfill and three subsequent soil layers. The finite element mesh of the concrete arch is composed of 64 elements. This discretization is

adequate to represent the arches compressive circumferential behavior.

The finite element mesh is extended in space so as to maximize the simulation time before any reflected waves from the finite element boundaries reach the shallow buried arch. Dashpots are placed at the boundaries to absorb any waves which are generated there.

For each test of the series, forced loading of the form $P = P_{max} \sin(\omega t)$ is applied at the drive point.

Direct integration in time of the equations of motion was performed using a time step interval of 60 microseconds. A total of 0.24 seconds of real time response was simulated.

The use of the advanced soil plasticity CAP model, which satisfies the requirements of continuity and uniqueness of solution and has the capability of simulating a wide range of real effects in soils was deemed essential for these analyses (Refs. 6, 7 and 8).

The CAP model is based on the classical incremental plasticity theory and is capable of representing the mechanical behavior of soils and rocks while satisfying all theoretical requirements for properly posed initial/boundary value dynamic problems. The proper use of the CAP model assures existence and uniqueness of solution as well as continuous dependence on the initial and boundary data. The CAP model has a non-softening convex yield surface. For stress points on the yield surface, the plastic strain rate vector is outwardly directed and normal to the yield surface in stress space. The CAP model permits inelastic hardening in hydrostatic loading, limits the amount of dilatancy during shear failure and provides a good fit to material property data.

To examine the interplay of the various components of the soil material nonlinearities, two different soil CAP models are used. They are;

1. Elasto-Plastic soil behavior (CAP Model)
2. Viscoelasto-Plastic soil behavior (Viscoelastic CAP)

These models will serve to isolate the role of soil non-linearities in determining the response of the arch structure in forced vibration testing.

2.2 VISCOELASTIC CAP MODEL.

Certain amendments to the CAP model were made to improve its capability to represent cyclic behavior characteristic of sinusoidal ground motions. Much of the previous use of the CAP model has been for ground shock calculations involving much higher stress levels than are applicable to low amplitude sinusoidally induced motions. Additionally, blast-induced loadings generally include a single peak compressive load followed by several smaller peaks. For these cases, any hysteresis in cyclic loading after the initial pulse is generally viewed as unimportant.

In vibration induced sinusoidal motion where cyclic shear is a predominant effect, hysteresis behavior caused by cyclic loading must be considered. In order to model this energy dissipation process, a viscoelastic stress-strain relation is incorporated into the CAP model to simulate the effects of low amplitude cyclic hysteresis within the yield surface. This allows for a controlled amount of energy dissipation in cyclic loading and can be fine tuned to provide the correct damping at the frequencies associated with the forcing functions.

Experimental results indicate that the amount of hysteresis for soils is relatively rate independent. Because of this experimental observation, the following approach, as discussed in detail in Reference (9) is taken;

Linear viscous damping is included to model stress paths within the yield surface of the CAP model. A standard solid is chosen to represent the shear behavior for stress paths within the current yield surface. This standard solid model requires three material parameters to describe the deviatoric viscoelastic response. These parameters are an instantaneous modulus G_f , a long term modulus G_s and a relaxation frequency ω .

The viscoelastic portion of the model is described by

$$\dot{s} + \omega s = 2G_f \dot{e}^E + 2\omega G_s e^E \quad (1)$$

where s and e^E are the stress and elastic strain deviators, ω is a relaxation frequency and G_f and G_s represent the shear moduli under fast and slow loading respectively.

The volumetric behavior is elastic

$$J_1 = 3K\epsilon_v^E \quad (2)$$

where J_1 and ϵ_v^E are the traces of the stress and strain tensors and K is the bulk modulus.

To obtain numerical values for these parameters an experimentally justified approximation is made that both the hysteresis and the average modulus are relatively frequency independent. The two parameters G_s and G_f are related to an average modulus over a loading cycle and to the energy loss per cycle at a central frequency of interest. The constants G_s and G_f can be obtained from a single load - unload curve of the compacted native backfill. The parameters G_s and G_f are related to the average modulus over the cycle and to the energy loss per cycle. The parameter ω is introduced, where is the circular frequency at which the energy loss per cycle of a standard solid reaches a maximum.

The parameter ω is chosen to correspond to the central frequency of interest, that is the forcing function frequency. Thus for the main frequency of interest, both the hysteresis and the average moduli are relatively frequency independent.

The viscoelastic algorithm begins by computing a viscoelastic "trial value" for the stresses, i.e., a value based on the assumption that no failure or cap plasticity occurs. If the assumption is found to be false, the stresses are revised by means of a "plastic correction" (Ref. 10).

For reasons of accuracy under arbitrary loading paths, the viscoelastic trial values are obtained for a strain increment $\Delta \epsilon$ during a time step Δt as the exact solution for linear straining during the time step $t_n \leq t \leq t_n + \Delta t$,

$$e^E(t) \approx e^{E_n} + \Delta e^E \left(\frac{t - t^n}{\Delta t} \right) \quad (3)$$

where $e^E(t)$ is the viscoelastic deviatoric strain at t_N . Substituting equation 3 into equation 1 produces

$$\dot{s} + \omega s = 2G_f \frac{\Delta e^E}{\Delta t} + 2\omega G_s \left[e^{E_n} + \frac{\Delta e^E}{\Delta t} (t - t^n) \right] \quad (4)$$

which may be solved using $s(t_n) = s^n$, to give

$$S(t) = S^n + 2G_s \frac{\Delta e^E}{\Delta t} (t - t^n) - \left[s^n - 2G_s e^{E_n} - 2 \frac{G_f - G_s}{\omega} \frac{\Delta e^E}{\Delta t} \right] \left[1 - e^{-\omega(t-t_n)} \right] \quad (5)$$

at $t = t_n + \Delta t$:

$$S^{n+1} = S^n e^{-\omega \Delta t} + 2G_s e^{E_n} (1 - e^{-\omega \Delta t}) + 2 \left[G_s + \frac{G_f - G_s}{\omega \Delta t} (1 - e^{-\omega \Delta t}) \right] \Delta e^E \quad (6)$$

which is the viscoelastic trial deviatoric stresses.

The viscoelastic trial stresses are then checked against the failure envelope and cap. If either or both of these surfaces is exceeded, the stress point is corrected so as to satisfy the appropriate yield condition and normal flow rule.

The viscoelastic model was fit to the available data for the backfill soil (Figure (3)).

The bulk modulus K was estimated from the uniaxial stress-strain properties of the compacted native backfill.

The "fast" and "slow" shear moduli, G_f and G_s , respectively were related to the size of the elliptic hysteresis loop and are dependent upon the amount of energy dissipated through viscous damping in the soil material.

The viscoelastic relaxation parameter ω is taken to be equal to the forced frequency of excitation of the structure.

For the backfill soil material, the properties used to fit the viscoelastic CAP model are estimated from the uniaxial stress-strain properties of the compacted native backfill (Fig. 3)

exhibiting a confined modulus ($K + 4/3 G$) of 26000 psi and are as follows:

$$K = 18000. \text{ psi}$$

$$G_s = 6000. \text{ psi}$$

$$G_f = 9000. \text{ psi}$$

$$C_W = 0.05$$

$$C_R = 3.0$$

$$C_A = 1.02 \text{ ksi}$$

$$C_B = 0.2 \text{ (1/ksi)}$$

$$C_C = 1.0 \text{ ksi}$$

$$C_D = 1.5 \text{ (1/ksi)}$$

$$E_L = 0.0 \text{ ksi}$$

$$LTYPE = 1$$

$$TCUT = .02 \text{ ksi}$$

$$FCUT = .02 \text{ ksi}$$

SECTION 3

RESULTS OF BURIED ARCH SIMULATION STUDIES

3.1 DISCUSSION OF RESULTS.

The physical results obtained from the ESSEX V buried structure tests differed appreciably in form from experimental predictions. In an attempt to explain the reasons for this difference, various damping mechanisms have been identified as possible causes of discrepancy between experimental and analytical results (Ref. 2). These damping mechanisms include:

1. Radiation damping
2. Interface friction between the soil and the structure
3. Hysteresis in the soil backfill adjacent to the structure
4. Structural damping

Previous work (Ref. 2) focused on the mechanisms of radiation damping and friction, as they were previously believed to be capable of being the major contributors to the total effective damping.

The present study focuses on the role of soil hysteresis in contributing to the total effective damping needed to suppress resonance. Soil hysteresis causes energy to be absorbed during the cycles of load-unload-reload produced by the driving force oscillations. The actual amount of effective hysteresis damping is a function of the amount of energy absorbed in each cycle.

Mechanical impedance data obtained from the ESSEX V test series showed the variation in impedance levels (F/V) due to changes in the forcing function frequency. Each trough in the impedance curve represents a frequency at

which resonance occurs and represents a natural frequency of the buried structure.

Analytical impedance results were obtained for the three test series which used a 500 pound (2224 N) forcing function. These series are;

1. A single vibrator at the arch's crown
2. Two vibrators in phase
3. Two vibrators out of phase

For each test series, a frequency sweep of 50 to 1000 hertz was experimentally performed.

The analytical simulation studies were performed for a frequency sweep from 50 to 250 hertz in intervals of 10 hertz. For each frequency in the interval, a direct integration in time was performed. That is, 21 separate time integration analyses were performed to obtain the frequency sweep. A more limited frequency range was used in the analytical studies versus the experimental studies because of limitations in the analytical procedure at both low (less than 50 hertz) and high (greater than 250 hertz) frequencies. The reasons for this are that in the low frequency range, the use of absorbing boundaries along the finite element mesh boundaries restricts the rigid body motion prevalent for these low frequencies, thereby invalidating the analytical procedure and for the high frequency range, the size of the finite element mesh restricts the frequency content of the solution, thereby invalidating the analytical procedure.

The simulation study considers a cross-section of the arch with length effects assumed to satisfy plane strain kinematics. The forcing function for the plane strain analyses is force per unit length of the arch (F/L). Therefore, the

analytically obtained impedance values differ from those measured. The analytical impedance values are obtained from $(F/L)/V$. The analytical impedance values differ in units from the experimental values by a inverse length unit. This discrepancy can be eliminated by assuming a characteristic length L^* for which the plane strain analyses impedance can compare with the full three dimensional response. A possible value for L^* could be the arch's radius. Then the analytical impedance values would be obtained from $(F/V)*(L^*/L)$.

To isolate the effects of soil hysteretic nonlinearity upon impedance versus forcing function frequency relations, results are presented for two assumed backfill soil models. The first soil model is an elastic-plastic CAP model and the second is a viscoelastic CAP model.

For the single vibration test, using a 500 lb (2224 N) force at drive point F1 (crown of arch), the effect of backfill soil hysteresis is illustrated in figure (4). For the case of elastic-plastic backfill soil model, two distinct troughs in the impedance curve are obtained. These occur at 100 and 180 hertz and represent frequencies where structural resonance occurs. However, the use of a viscoelastic-plastic backfill model suppresses the resonance occurring at 180 hertz and smooths out the impedance trough which occurs at 100 hertz. Thus the use of a viscoelasticity backfill CAP model reduces the tendency of the structural arch to resonate within the frequency band considered.

The comparisons of both analytical results with the experimental data for the single vibration test are shown in figures 5 and 6. The experimental response of the two gages, CL6 and CL8 are shown. The response of the gages CL6 and CL8 illustrate the change in impedance along the length of the arch's crown. If the arch responded in plane strain modes, these two gages should have identical responses. This is not observed as gage CL8 has a greater

impedance than gage CL6 because it is further removed from the force drive point. For the elastic backfill soil model, the computed resonance at 180 hertz is not observed in the experiment at either of the measured gages. For the viscoelastic (hysteretic) backfill soil model, the computed response shows a resonance at 90 hertz. A resonance of 80 hertz is exhibited by gage CL8. Note that the magnitude of the calculated response differs from the magnitude of the measured response because of the analytical assumption of plane strain response. What is critical, however, is that the inclusion of a hysteretic backfill soil model alters the shape of the response impedance diagram by suppressing the resonance mode at 180 hertz.

For the dual in-phase vibration test, using a 500 lb (2224 N) force at drive points F2 and F3, the effect of backfill soil hysteresis is illustrated in Figure (7). For the case of elastic-plastic backfill soil, a distinct trough in the impedance curve is obtained. This occurs at 140 hertz and represents structural resonance. The use of a viscoelastic-plastic backfill soil model does not suppress the resonance occurring at 140 hertz.

The comparisons of both analytical results with the experimental data for the dual in-phase vibrator test are shown in Figures (8) and (9). The experimental response of the gage A3 is shown. Note that the magnitude of the computed impedance curve differs from the magnitude of the measured response because of the plane strain limitation. As seen in Figure (7), the inclusion of the hysteretic soil model did not suppress the calculated resonance mode at 140 hertz. This resonance mode was not observed in the experimental records.

For the dual out-of-phase vibrator test, using a 500 lb (2224 N) force at drive points F2 and F3, the effect of backfill soil hysteresis is illustrated in Figure (10). For the case of elastic-plastic backfill soil, a distinct trough in the impedance curve is obtained. This occurs at 110 hertz and represents a frequency where structural resonance occurs. However, the use of a viscoelas-

tic-plastic backfill soil model suppresses the resonance occurring at 110 hertz. Thus the use of a viscoelastic backfill CAP model reduces the tendency of the structural arch to resonate within the frequency band considered.

The comparisons of both analytical results with the experimental data for the dual out-of-phase vibrator test are shown in Figures (11) and (12). The experimental response of gage A3 is shown. For the elastic backfill soil model, the computed resonance at 110 hertz is not observed in the experiment gage record. For the viscoelastic (hysteretic) backfill soil model, the computed response suppresses the resonance at 110 hertz. The inclusion of a hysteretic backfill soil model alters the shape of the response impedance diagram by suppressing the resonance mode at 110 hertz.

For the single vibrator test and the dual out-of-phase vibrator test, the inclusion of viscoelasticity into the backfill soil model served to suppress resonant modes. The suppression of these resonance modes agreed with the experimental data which showed that for the arch structure, resonance was suppressed in the covered tests as compared to the uncovered tests.

For the dual in-phase vibrator test, the inclusion of viscoelasticity into the backfill soil model did not serve to suppress the resonant modes. This suppression was observed however in the experimental gage records. Possibly, the reason for this difference is that the plane strain assumptions were not at all valid for this in-phase test series.

SECTION 4

CONCLUSIONS AND RECOMMENDATIONS

4.1 CONCLUSIONS.

1. Resonant frequencies for the covered arch with a single vibrator force at drive point F1 are analytically suppressed when a viscoelastic-plastic soil backfill CAP model is used.
2. Resonant frequencies for the covered arch with a dual out-of-phase vibrator force at drive points F2 and F3 are analytically suppressed when a viscoelastic-plastic soil backfill CAP model is used.
3. Resonant frequencies for the covered arch with a dual in-phase vibrator test at drive points F2 and F3 are not analytically suppressed when a viscoelastic-plastic soil backfill CAP model is used.
4. The inclusion of a viscoelastic-plastic soil model is critical in helping to explain the resonant mode suppression

observed in the covered arch experimental results.

5. Impedance testing excites nonlinear soil response typified by hysteretic energy losses and radiation and friction energy dissipation.
6. The applicability of impedance testing to define buried arch response is questionable.

4.2 RECOMMENDATIONS.

Additional experimental and analytical studies are needed to expand the data base of buried structural response. Soil parameters defining hysteretic energy losses need to be more accurately defined to assist in establishing viscoelastic-plastic soil constitutive models to simulate the hysteretic energy losses which occur during the forced vibration tests of buried structures.

SECTION 5

REFERENCES

1. Crowson, Roger D. , "ESSEX-Diamond Ore Research Program: Vibration test and analyses of ESSEX V Model Structures". Weapons Effects Laboratory, U.S. Army Engineer Waterways Experiment Station, WES TR N-78-2, August 1978.
2. Isenberg, J. , Levine, H.S. and Pang, S.H., "Numerical Simulation of Forced Vibration Tests on a Buried Arch". Weidlinger Associates Contract No. DNA 001-76-C-0110, Report No. DNA 4281F, Defense Nuclear Agency, 1977.
3. Merkle, D.H. and Merkle, L.D., "High Frequency Analysis of Circular Arches," Applied Research Associates Inc. Contract No. F29601-85-C-0029, Report No. AFWL-TR-86-22 , Air Force Weapons Lab, 1986.
4. Wojcik, G. and Isenberg, J., "Effects of Radiation Damping on Vibration of a Shallow-Buried Rectangular Structure," Weidlinger Associates Contract No. DNA 001-77-C-0233, Report No. DNA 4600F , Defense Nuclear Agency, 1978.
5. Daddazio, R.P. , Ettouney, M. and Sandler, I., "Nonlinear Dynamic Slope Stability Analysis," Journal of Geotechnical Engineering , ASCE Vol. 113, No. 4, pp. 285-298, (1987).
6. DiMaggio, F.L. and Sandler, I.S., "Material Model for Granular Soils," Journal of the Engineering Mechanics Division, ASCE, Vol. 97, No. EM3, pp. 935-949, (1971).
7. Sandler, I.S., DiMaggio, F.L. and Balardi, G.Y., "Generalized Cap Model for Geological Materials, " Journal of the Geotechnical Division, ASCE, Vol. 102, No. GT7, pp. 683-699 (1976).
8. Sandler, I.S., "The Cap Model for Static and Dynamic Problems," Site Characterization - U.S. Symposium on Rock Mechanics, W.S. Brown, ed., University of Utah, Salt Lake City, Utah, pp.1A2-1 - 1A2-11, (1976).
9. Sandler, I.S. and Daddazio, R.P., "Analysis of Earthquake Induced Slope Failures" Phase 1 Technical Report, NSF July 1988.
10. Sandler, I.S. and Rubin, D., "An Algorithm and a Modular Subroutine for the Cap Model," International Journal for Numerical and Analytical Methods in Geomechanics, Vol. 3, pp. 173-186, (1979).

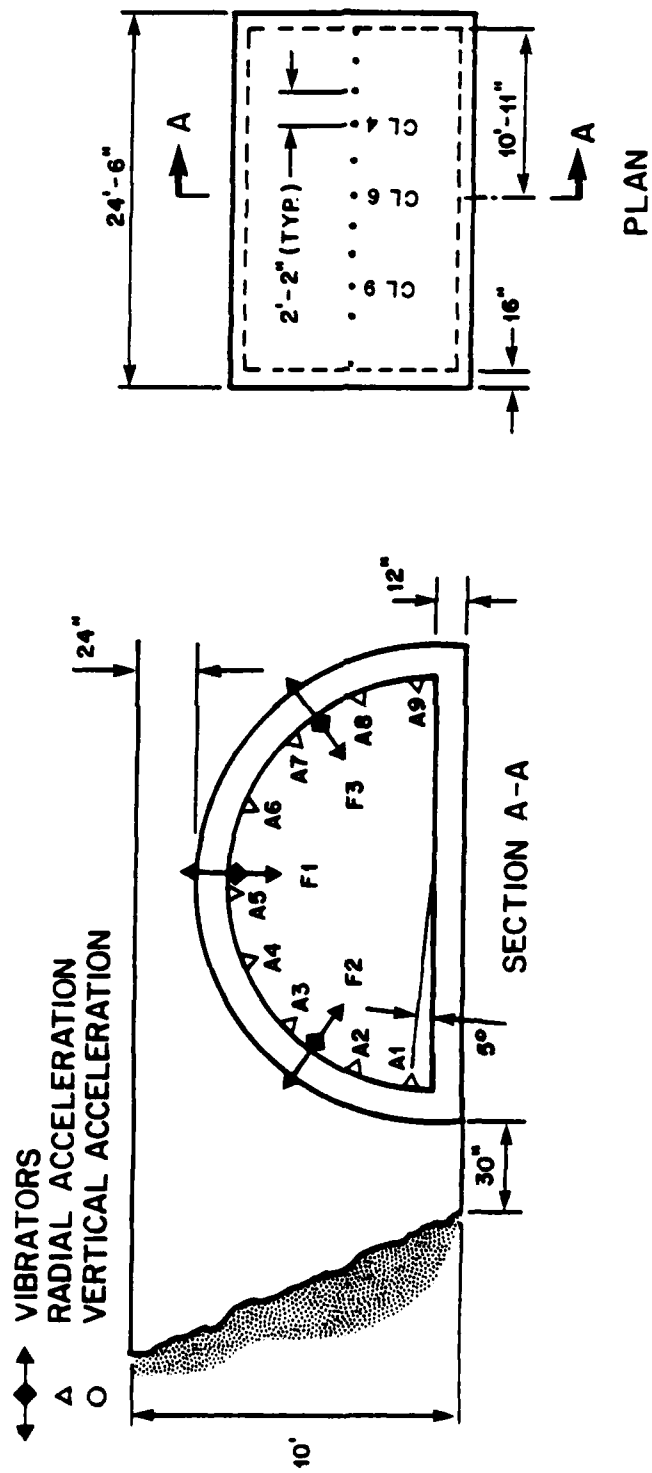


Figure 1. Geometry and instrumentation for arch structure.

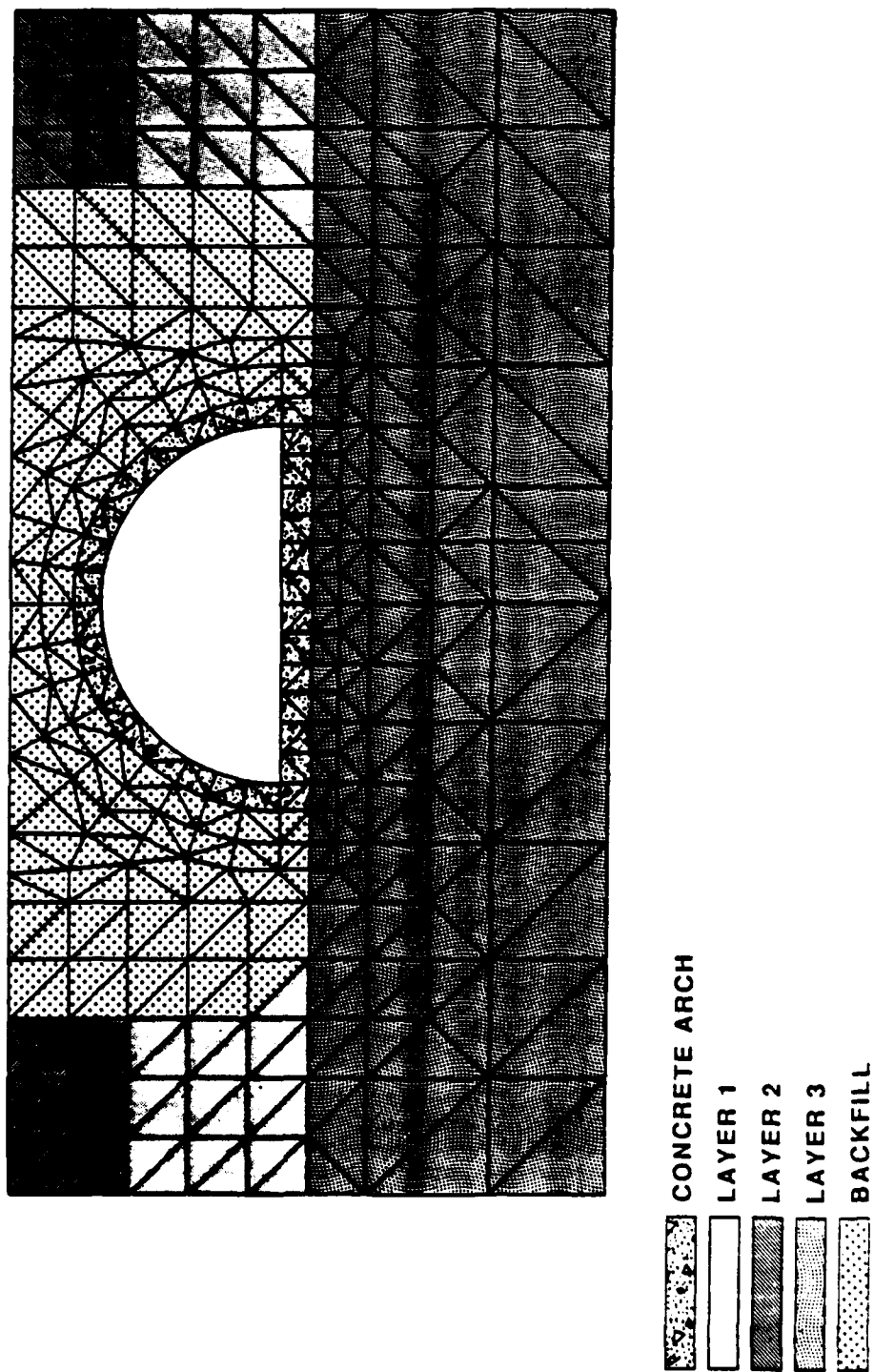


Figure 2. Finite element model of buried arch.

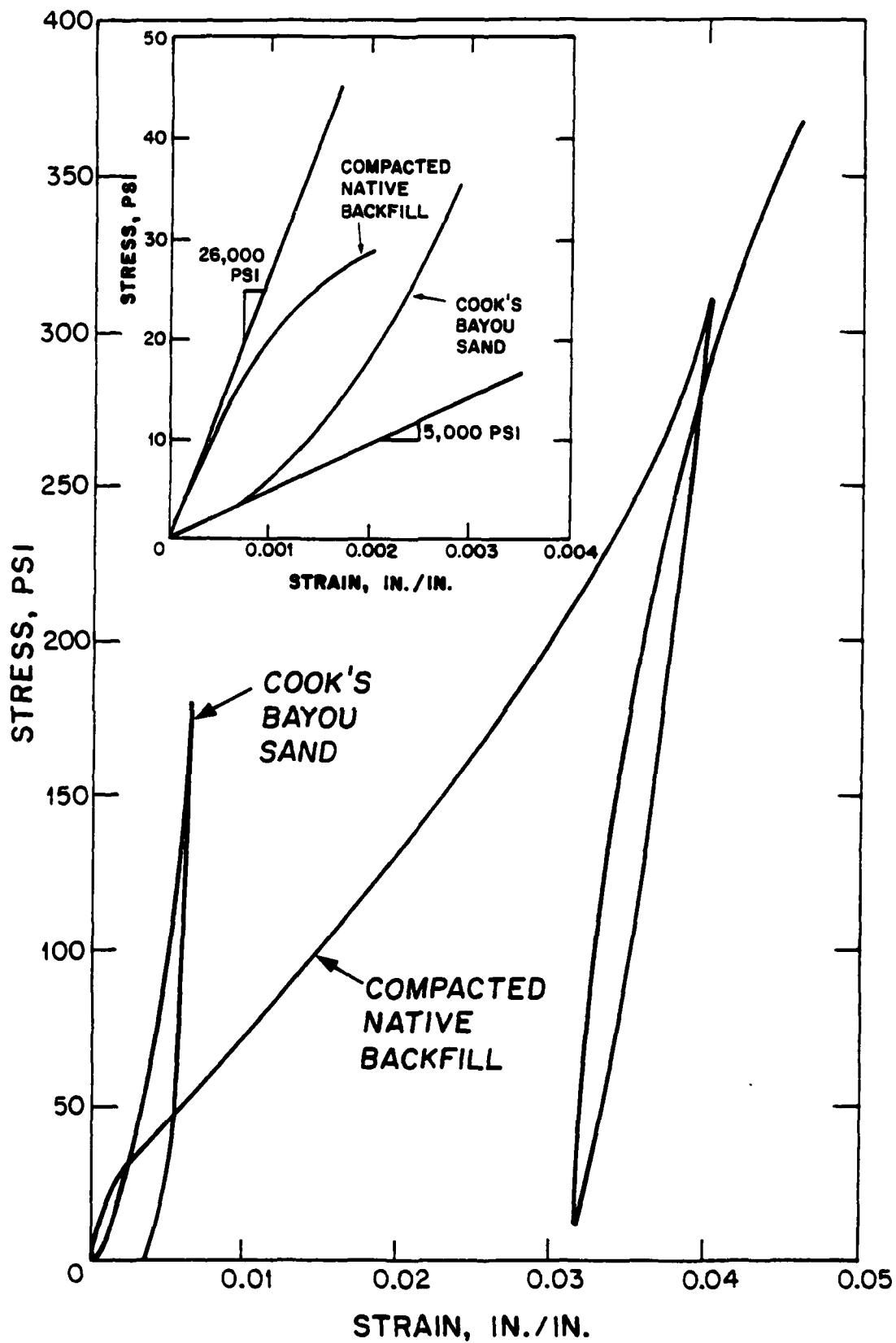


Figure 3. Uniaxial stress-strain properties of compacted native backfill ESSEX V arch.

MECHANICAL IMPEDANCE INFLUENCE OF SOIL HYSTERESIS

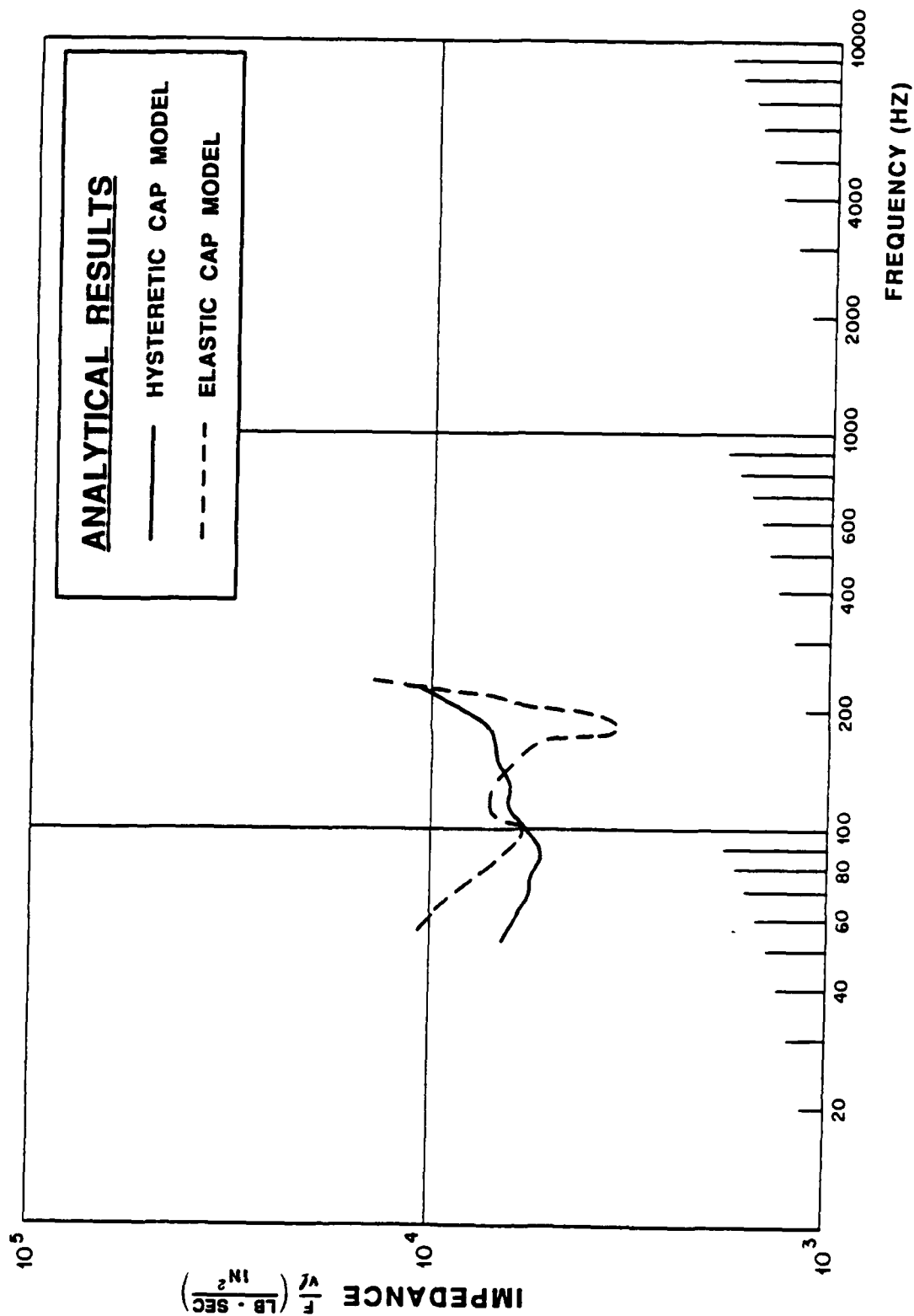


Figure 4. ARCH structure 3A, analytical response at crown - single vibration test,
F1 = 500 lbs (2224 N)

MECHANICAL IMPEDANCE EXPERIMENTAL VS. ANALYTICAL

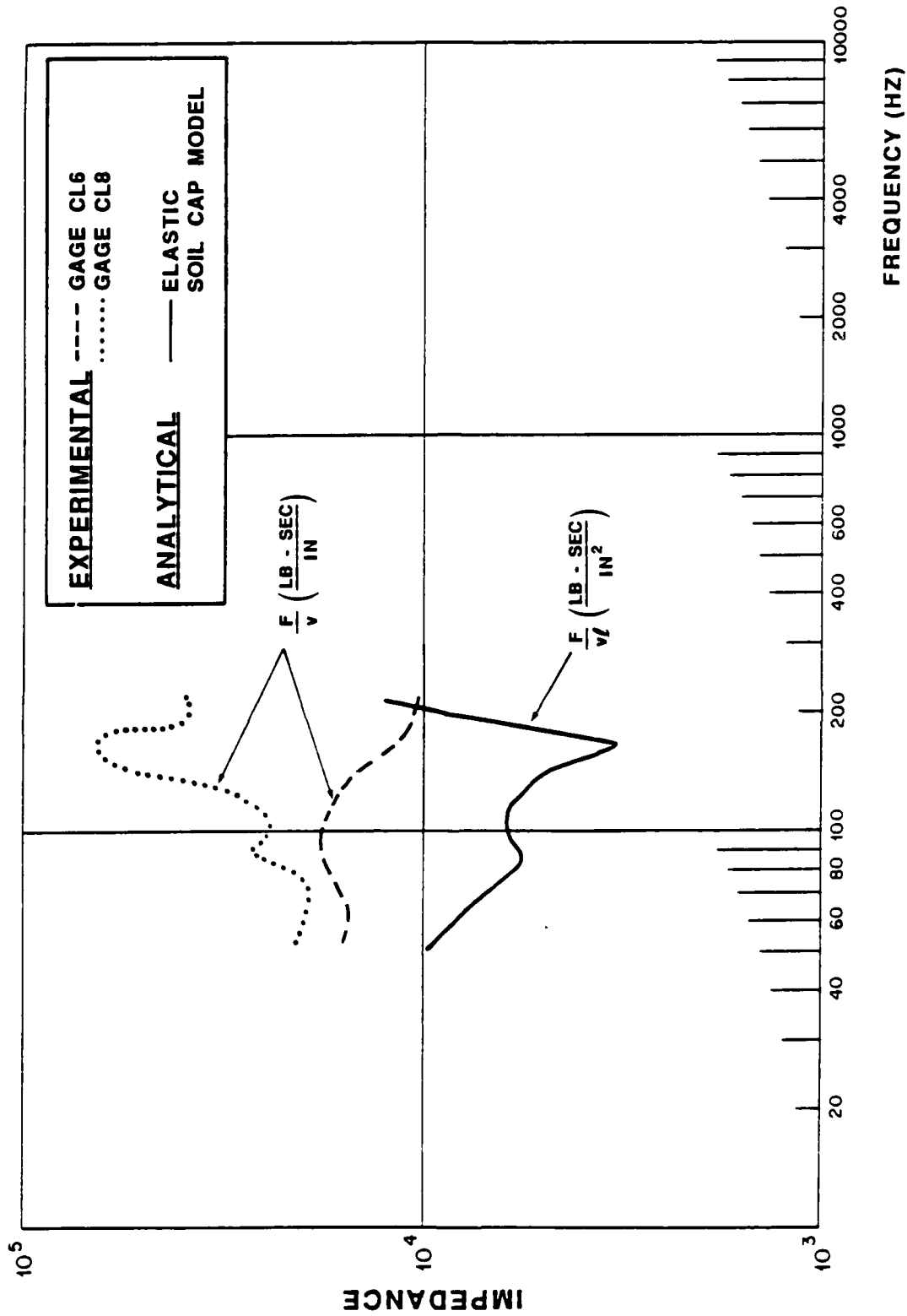


Figure 5. Elastic soil cap model - ARCH structure 3A,
analytical response at crown - single vibration test,
F1 = 500 lbs (2224 N).

MECHANICAL IMPEDANCE EXPERIMENTAL VS. ANALYTICAL

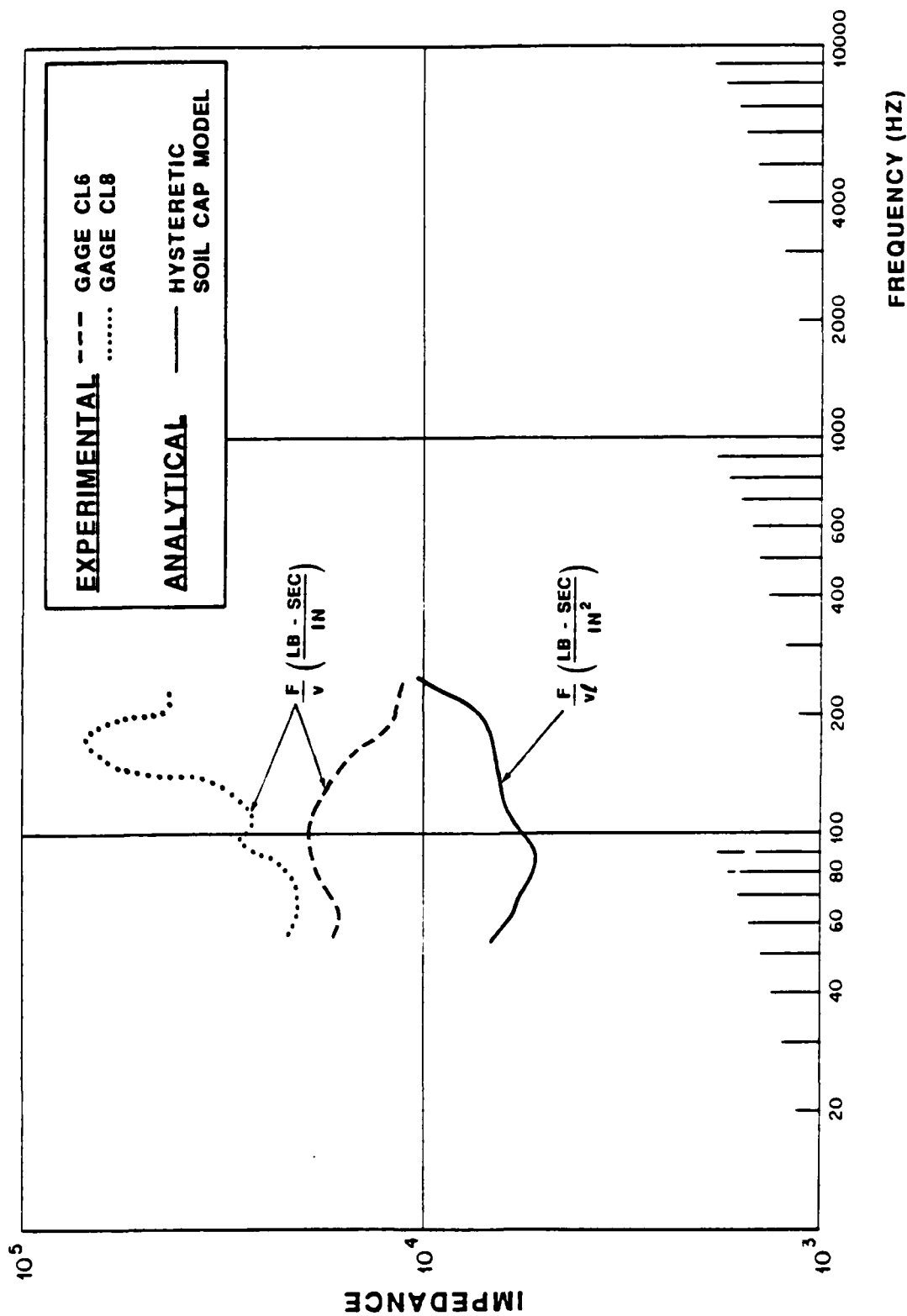


Figure 6. Hysteretic soil cap model - ARCH structure 3A, analytical response at crown - single vibration test, $F1 = 500 \text{ lbs (2224 N)}$.

MECHANICAL IMPEDANCE INFLUENCE OF SOIL HYSTERESIS

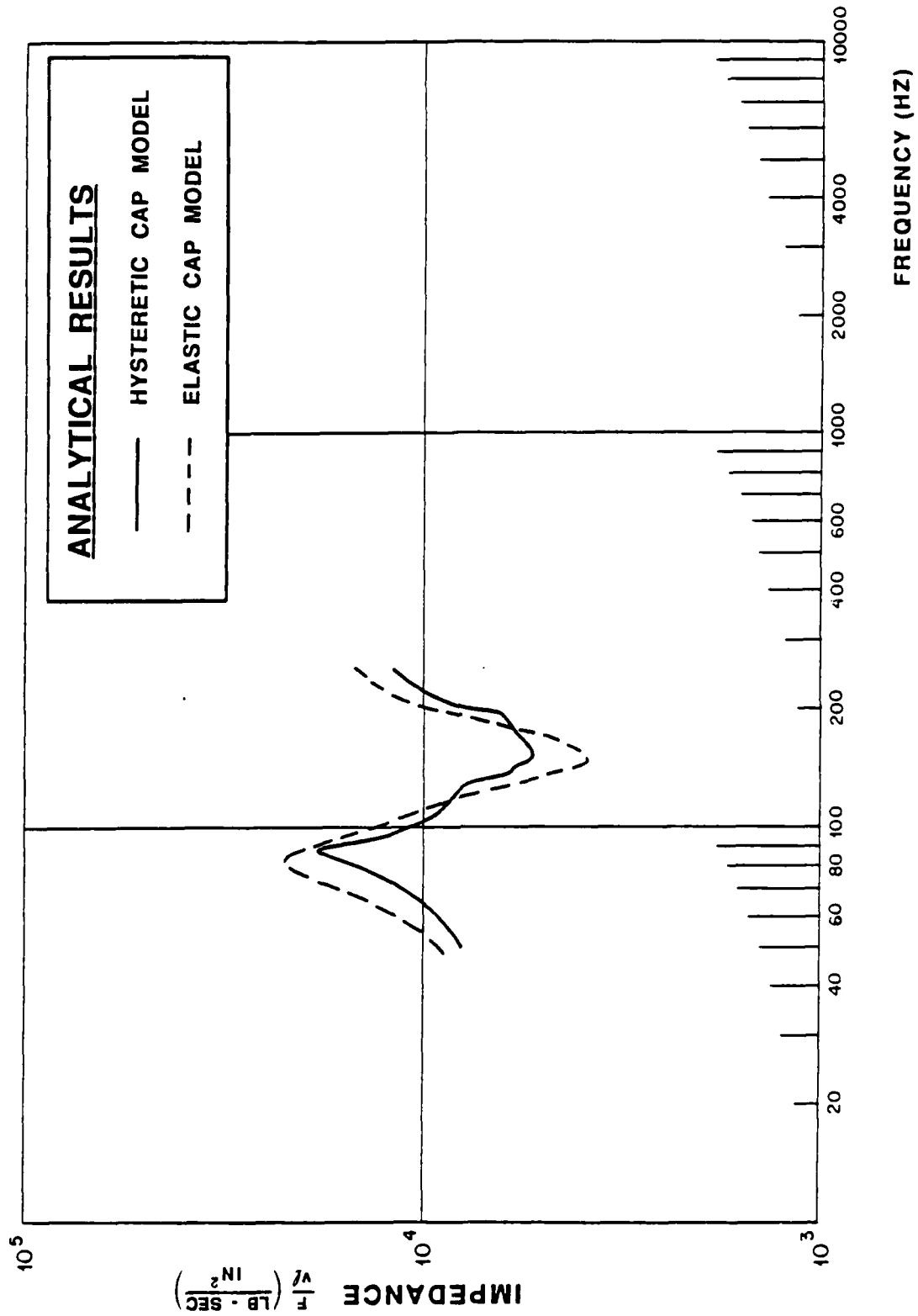


Figure 7. ARCH structure 3A, analytical response at gage location A3, single vibration test, $F1 = 500$ lbs (2224 N).

MECHANICAL IMPEDANCE EXPERIMENTAL VS. ANALYTICAL

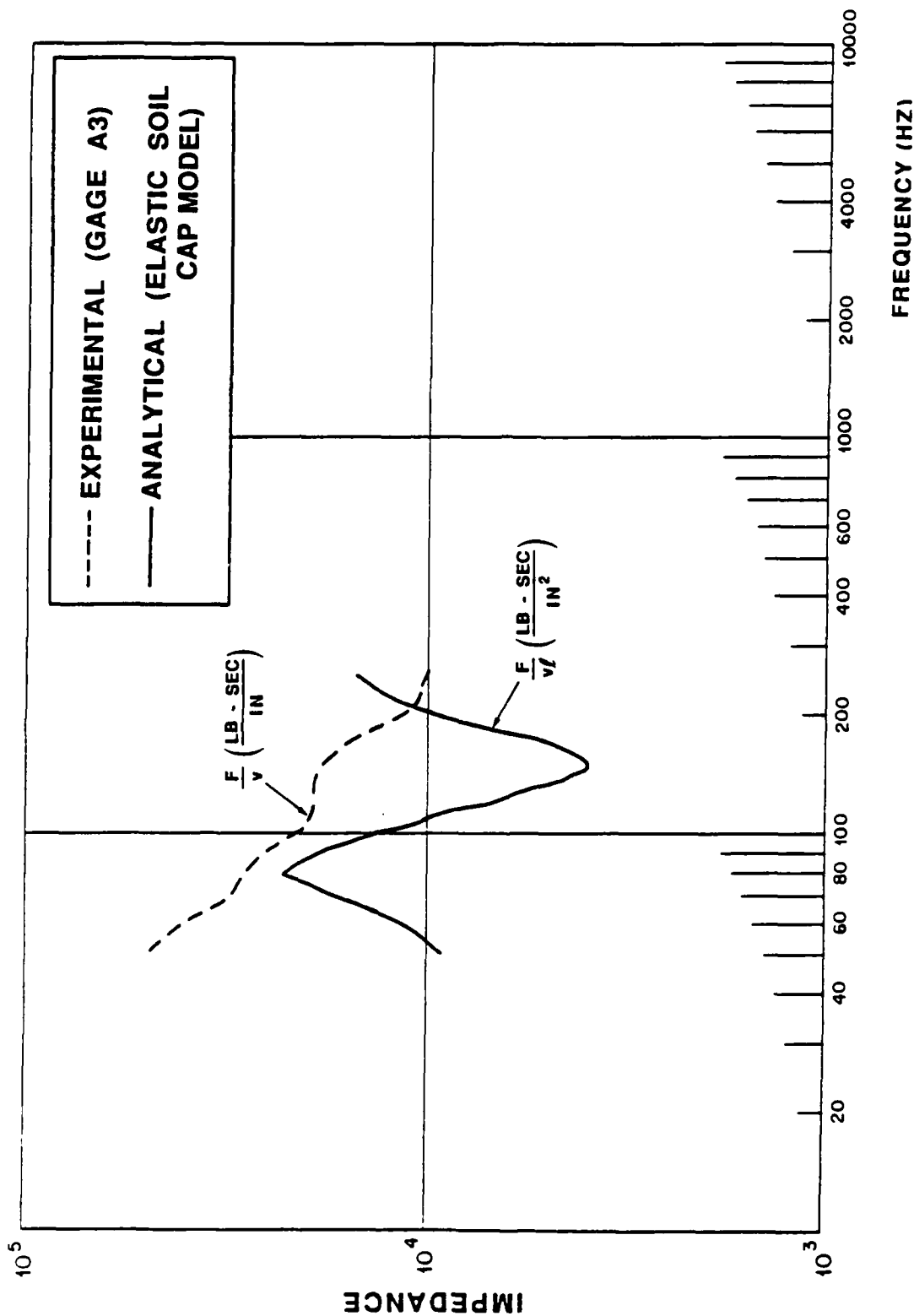


Figure 8. Elastic soil cap model - ARCH structure 3A, response data at gage A3 - two vibrators in phase, F2 = F3 = 500 lbs (2224 N).

MECHANICAL IMPEDANCE EXPERIMENTAL VS. ANALYTICAL

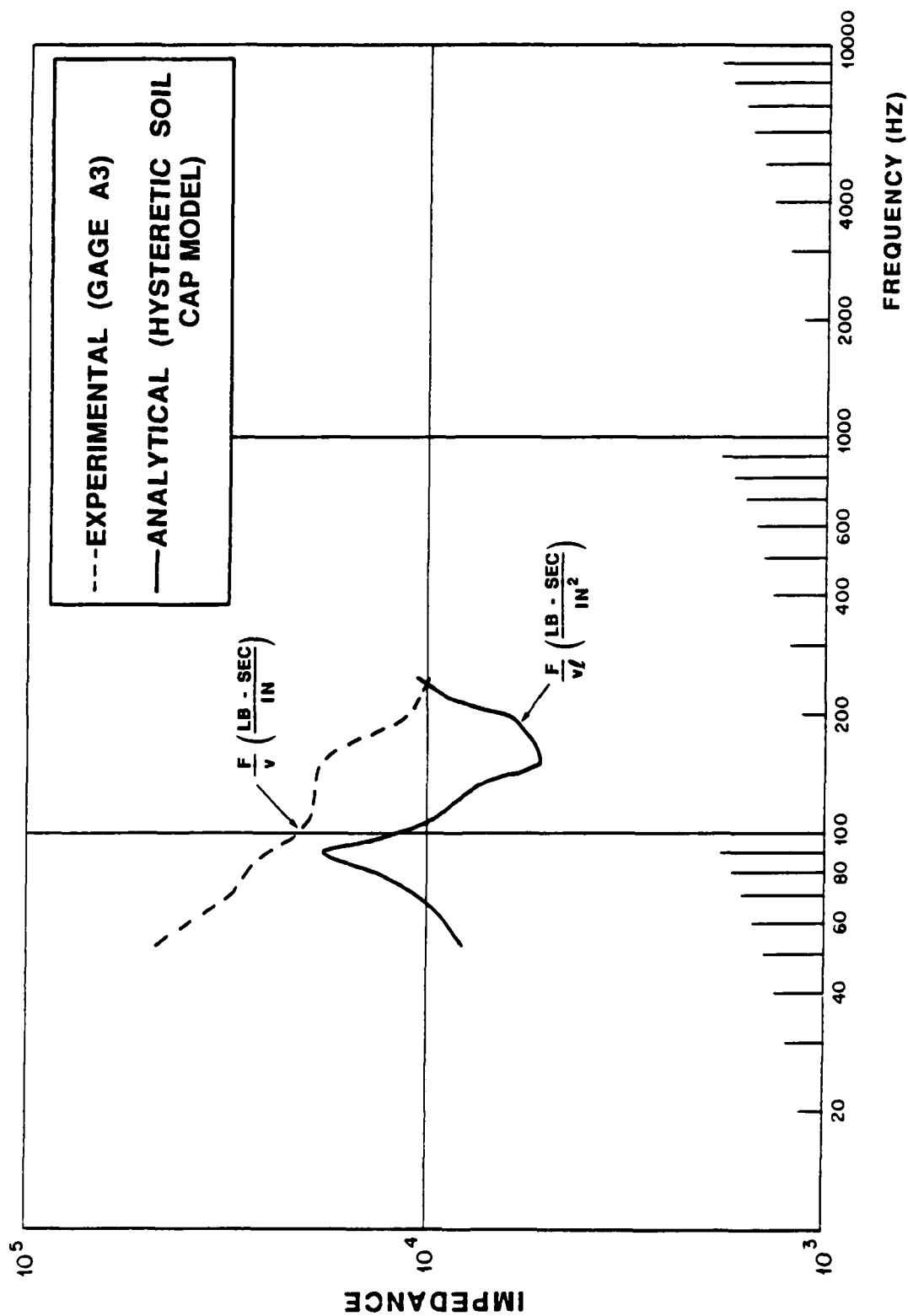


Figure 9. Hysteretic soil cap model - ARCH structure 3A,
response data at gage A3 - two vibrators in phase,
F2 = F3 = 500 lbs (2224 N).

MECHANICAL IMPEDANCE INFLUENCE OF SOIL HYSTERESIS

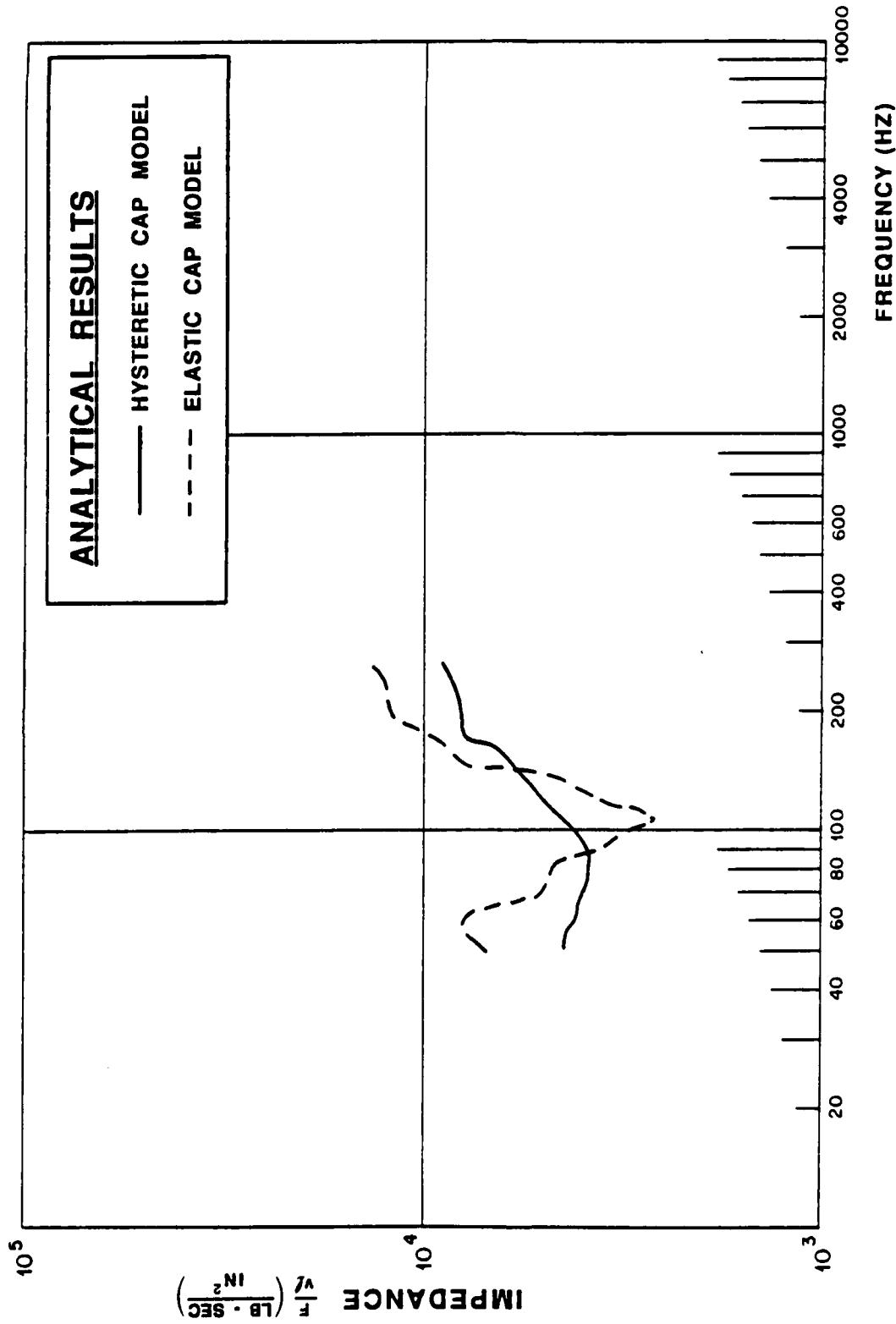


Figure 10. ARCH structure 3A, analytical response at gage location A3, two vibrators out of phase, F2 = F3 = 500 lbs (2224 N).

MECHANICAL IMPEDANCE INFLUENCE OF SOIL HYSTERESIS

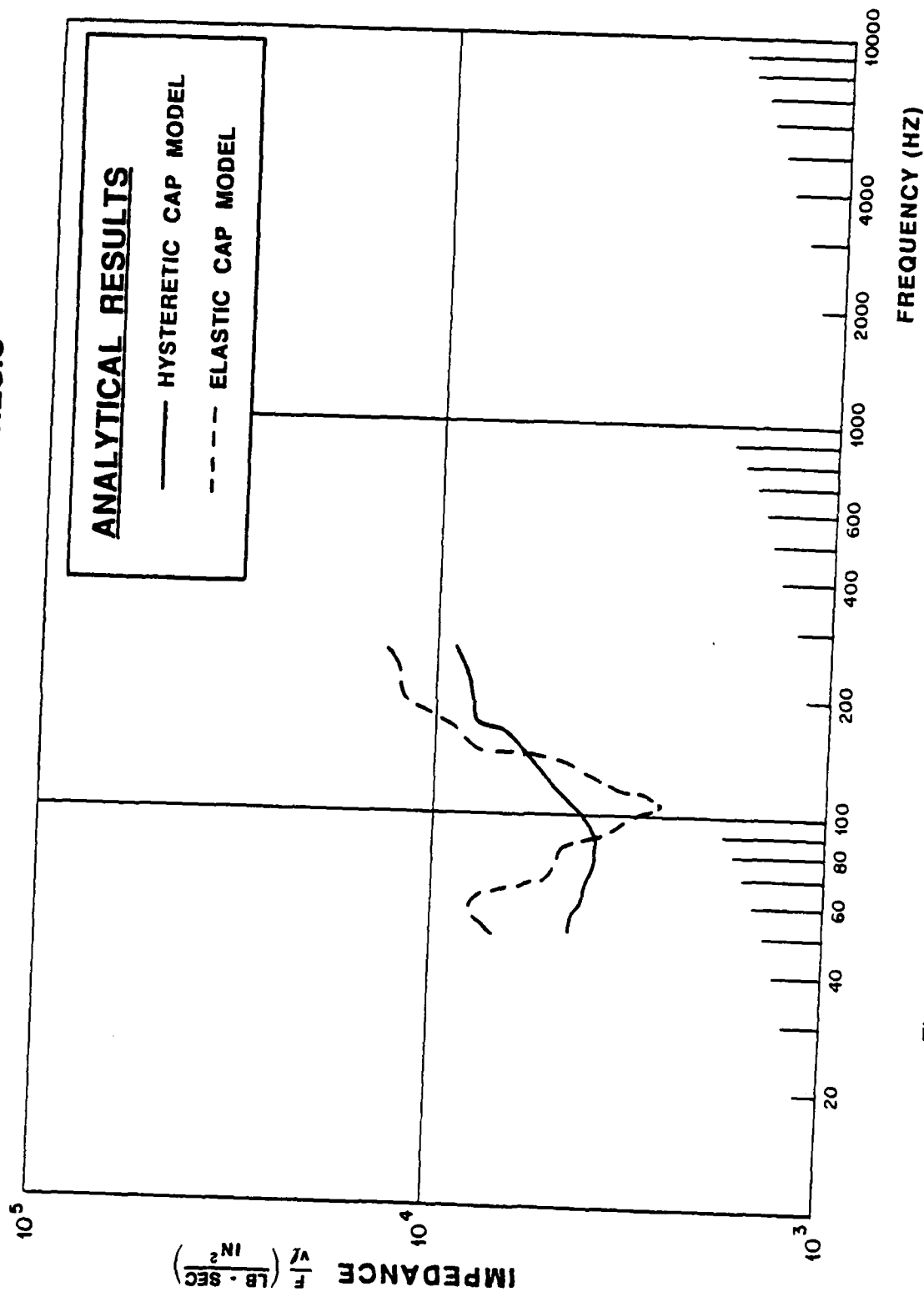


Figure 10. ARCH structure 3A, analytical response at gage location A3, two vibrators out of phase, $F2 = F3 = 500 \text{ lbs (2224 N)}$.

MECHANICAL IMPEDANCE EXPERIMENTAL VS. ANALYTICAL

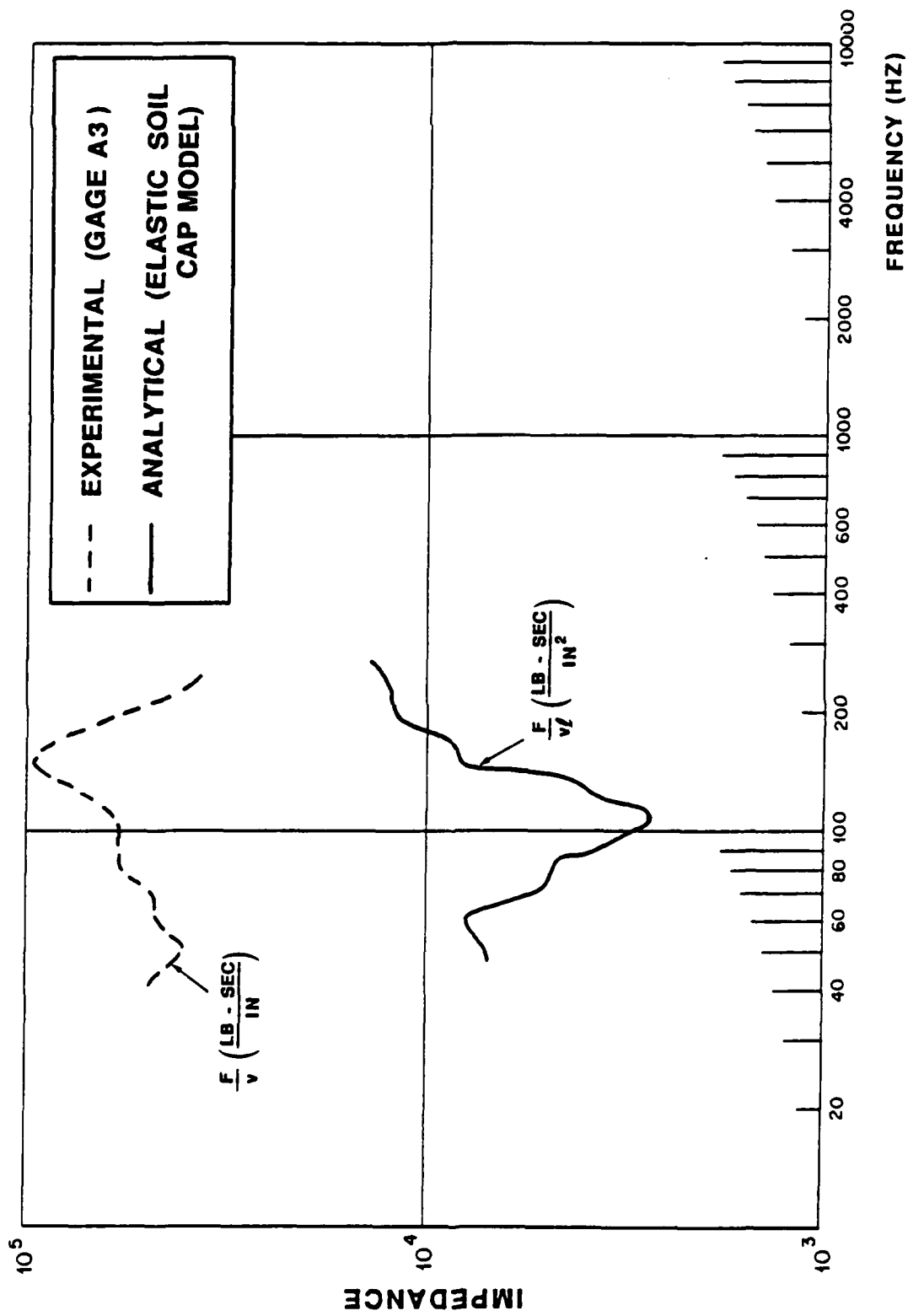
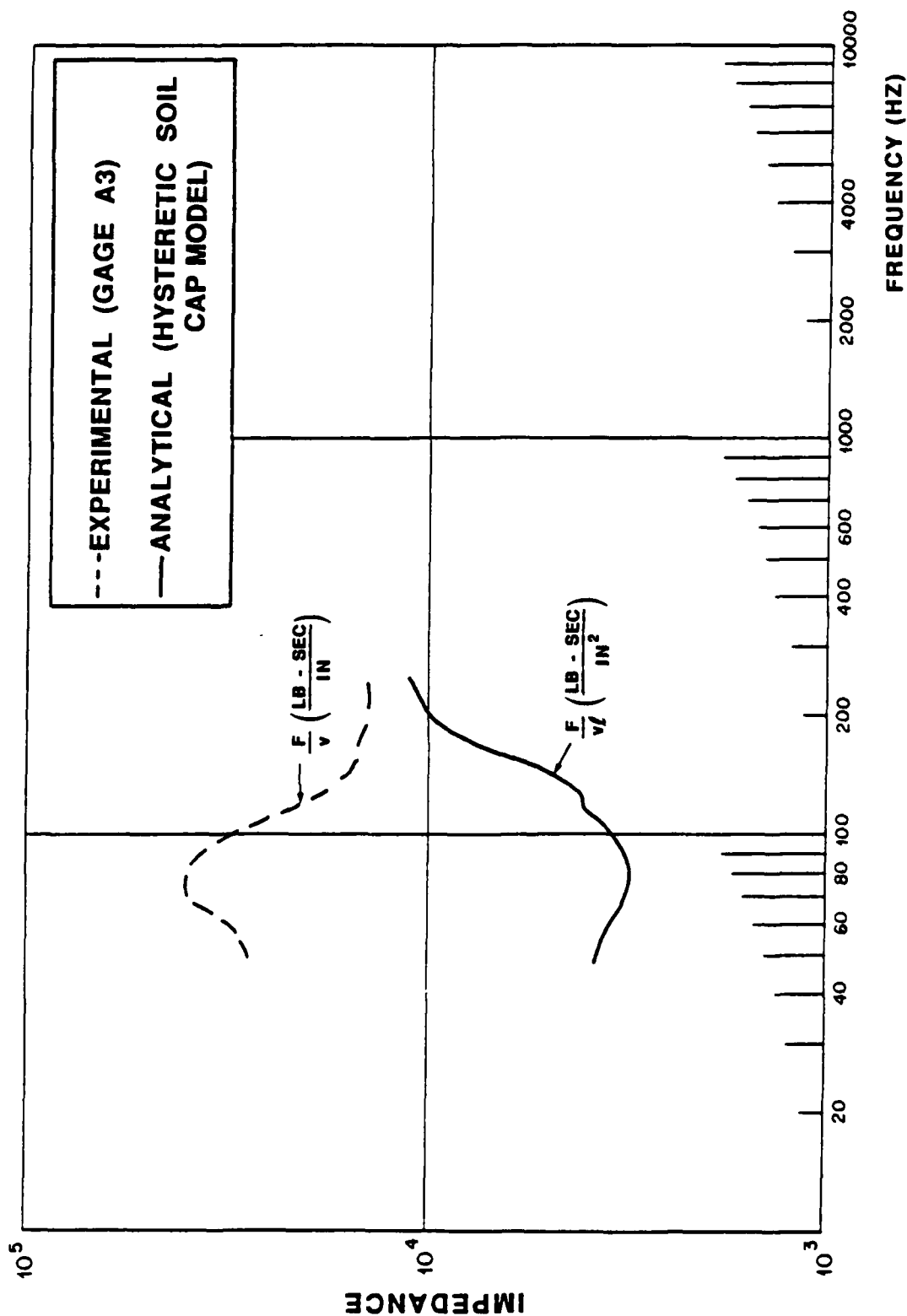


Figure 11. Elastic soil cap model - ARCH structure 3A,
response data at gage A3 - two vibrators out of phase test,
F2 = F3 = 500 lbs (2224 N).

MECHANICAL IMPEDANCE EXPERIMENTAL VS. ANALYTICAL



NOTATION

CA, CB CC, CD, CW, FCUT, TCUT CAP fit Parameters

e^E elastic strain deviator

ϵ_v^E trace of strain tensor

F_{MAX} maximum harmonically applied force

G_f shear modulus under fast loading

G_s shear modulus under slow loading

J_1 trace of stress tensor

K bulk modulus

S stress deviator

v_{MAX} maximum velocity

ω relaxation frequency

DISTRIBUTION LIST

DNA-TR-88-212

DEPARTMENT OF DEFENSE

ASSISTANT TO THE SECRETARY OF DEFENSE
ATOMIC ENERGY

ATTN: EXECUTIVE ASSISTANT

DEFENSE INTELLIGENCE AGENCY

ATTN: RTS-2B

DEFENSE NUCLEAR AGENCY

ATTN: SPWE/MAJ WADE

ATTN: SPSP

ATTN: TDTR

4 CYS ATTN: TITL

DEFENSE NUCLEAR AGENCY

ATTN: TDNM

2 CYS ATTN: TDTT W SUMMA

DEFENSE TECHNICAL INFORMATION CENTER

2 CYS ATTN: DTIC/FDAB

STRATEGIC AND THEATER NUCLEAR FORCES

ATTN: DR E SEVIN

THE JOINT STAFF

ATTN: J-5 NUCLEAR & CHEMICAL DIV

ATTN: JAD/SFD

ATTN: JAD/SSD

ATTN: J8 NUCLEAR FORCE ANALYSIS DIV

DEPARTMENT OF THE ARMY

DEP CH OF STAFF FOR OPS & PLANS

ATTN: DAMO-NCZ

HARRY DIAMOND LABORATORIES

ATTN: SLCHD-NW-P

U S ARMY BALLISTIC RESEARCH LAB

ATTN: SLCBR-SS-T

ATTN: SLCBR-TB-B G BULMASH

U S ARMY NUCLEAR & CHEMICAL AGENCY

ATTN: MONA-NU

U S ARMY NUCLEAR EFFECTS LABORATORY

ATTN: ATAA-TDC R BENSON

DEPARTMENT OF THE NAVY

NAVAL RESEARCH LABORATORY

ATTN: CODE 2627

ATTN: CODE 4770 G COOPERSTEIN

ATTN: CODE 7920 A WILLIAMS

NAVAL WEAPONS EVALUATION FACILITY

ATTN: CLASSIFIED LIBRARY

OFC OF THE DEPUTY CHIEF OF NAVAL OPS

ATTN: OP 654

DEPARTMENT OF THE AIR FORCE

AIR UNIVERSITY LIBRARY

ATTN: AUL-LSE

BALLISTIC SYSTEMS DIVISION

ATTN: ASMS

ATTN: MYE

WEAPONS LABORATORY

ATTN: NTA A SHARP

DEPARTMENT OF DEFENSE CONTRACTORS

KAMAN SCIENCES CORP

ATTN: DASIAC

KAMAN SCIENCES CORPORATION

ATTN: DASIAC

LACHEL PIEPENBURG AND ASSOCIATES

ATTN: D PIEPENBURG

PACIFIC-SIERRA RESEARCH CORP

ATTN: H BRODE

WEIDLINGER ASSOCIATES, INC

2 CYS ATTN: R S ATKATSH